Determination of high-frequency attenuation characteristic of coda waves in the central region of Nepal Himalaya

*Thakur Prasad Kandel[1], Masumi Yamada[2], and Prakash Pokhrel[1]

[1]Department of Mines and Geology, Lainchour, Kathmandu, Nepal
[2]Disaster Prevention Research Institude, Kyoto University, Japan
* Corresponding author's email: thakurkndl@gmail.com

ABSTRACT

The high-frequency coda wave attenuation in the central region of Nepal, in and around the Kathmandu valley, is estimated using vertical component seismograms of local earthquakes recorded at 16 different seismic stations of NAMASTE array. The estimated result is expressed in terms of Q_c, quality factor (inverse of coda wave attenuation). The value of coda quality factor (Q_c) is estimated at eight central frequencies of 1.5, 3.0, 6.0, 9.0, 12.0, 15.0, 18.0, and 21.0 Hz through four different coda window length from 20 to 50 s at 10 s interval by using the single backscattering model. The value of coda Q_c obtained from this study, shows a clear dependence on a frequency according to the power relation, $Q_c(f) = Q_0 f^n$, where Q_0 is Q_c at 1 Hz, and f is frequency and n represents the degree of frequency dependence. The mean value of Q_c of 16 different seismic stations was obtained as $(110 \pm 10.6) f^{1.03 \pm 0.03}$ at 30 s coda window length, which represents the high attenuation characteristics of the study area, and attenuation decreases with increasing central frequency. Q_0 increases from 73.1 ± 10.1 to 156.1 ± 13.6 and n decreases from 1.12 ± 1.05 to 0.92 ± 0.03 when the coda window length increases from 20 to 50 s. It is concluded that the study area is tectonically very active, highly heterogeneous, and heterogeneity decrease with depth. The coda Q obtained in this study is compatible with the result obtained in the region having a similar tectonic setting.

INTRODUCTION

Seismic waveforms recorded on sensors contain integrated information on the earthquake source, path attenuation, site amplification, (Stein and Wysession, 2009), and the instrument response. When the earthquake occurred, the seismic energy spreads in the form of a spherical waveform from origin to the earth's surface throughout the medium. High-frequency seismic wave (body waves, surface wave, and coda wave) attenuation is directly related to the geometrical structure (tectonic) and strength of the propagating media. The seismic wave attenuation and its spatial variation are important for understanding the crustal structure, which affects the ground motion prediction equations. The seismic wave energy decreases while propagating through media due to intrinsic attenuation, geometrical spreading, and scattering (Stein and Wysession, 2009).

Coda waves are not direct wave coming from earthquake source but are backscattered waves generated due to present of medium heterogeneity (Aki, 1969, 1980; Aki and Chouet, 1975) that appears after the arrival of body wave, the tail of a seismogram,

coming after direct S wave, can be identified as S coda wave or simply coda waves (Aki and Chouet, 1975; Sato, 1977). Coda wave attenuation is caused by two types of effects scattering and intrinsic attenuation, dependent on frequency. High-frequency dependence of coda attenuation is observed for more than 30 Hz (Kanao and Ito, 1991; Sato et al., 2012). The coda waves in the local event, epicenter distance up to 100 km (less than twice the Moho depth), their power spectra, and coda duration are relatively independent of focal distance (Aki and Chouet, 1975). Coda waves are widely used to estimate the attenuation characteristics of a different region of the world (e.g., Aki 1969; Pulli, 1984; Canas et al., 1995; Gupta et al., 1995, 1998; Havskov et al., 1989; Kanao and Ito, 1991; Kosuga, 1992; Paul et al., 2003; Kumar et al., 2005; Tripathi et al., 2012; Naghavi et al., 2017). Coda wave attenuation is not well studied in Nepal Himalaya, but several studies have been carried out in adjacent regions of Nepal Himalaya.

In this study, the coda wave attenuation characteristic of the central part of the Nepal Himalaya was estimated at 8 different central frequencies (Table 1) and 4 different coda window lengths from 20 to 50 s

by using the single backscattering method of Aki and Chouet (1975). This method is valid for signals that arrive long after the primary waves. The coda wave amplitude decreases with lapse time at a particulate frequency due to seismic energy attenuation and geometrical spreading. It is independent of the earthquake source, path effects, and site amplification (Aki, 1969). For that, we selected good quality seismograms from the aftershocks of the 2015 Gorkha earthquake. The frequency-dependent relationships for have been estimated at 16 stations in the central region of Nepal Himalaya. The present study of coda wave attenuation in the central region will enhance our knowledge about the regional seismic coda wave attenuation characteristics of the seismic and tectonically active region.

Table 1. Different central frequency components of the Butter worth band pass filter with law and high cutoff frquenc in Hz.

Low cutoff	Central Frequency	Hight Cutoff
1	1.5	2
2	3	4
4.5	6	7.5
6	9	12
8	12	16
10	15	20
12	18	24
14	21	28

GEOLOGY AND SEISMOTECTONIC IN THIS REGION

Nepal Himalaya lies in the central part of the Himalayan arc that is considered a result of a continent-continent collision process between Indian and Eurasian plates (Molnar and Tapponnier, 1975). The Himalaya, the highest mountain range of the world, represents an active collision orogeny combining crustal shortening and thickening, and that causes frequent strong earthquakes (Avouac, 2003). Our study area, the central region of Nepal Himalaya, is dominated by three north dipping major thrust systems: the Main Central Thrust (MCT), the Main Boundary Thrust (MBT), the Main Frontal Thrust (MFT) from north to south (Fig. 1 a and b). These are considered as root in-depth in a low angle decollement, called Main Himalaya Thrust (MHT), which produces most of the crustal deformation in the Himalaya (Cattin and Avouac, 2000).

The rocks of central Nepal are differentiated into the Nawakot Complex, representing the Lesser Himalayan sequence and the physically overlying Kathmandu complex (Stocklin and Bhattarai, 1977) belonging to the Higher Himalayan crystalline and Tethyan sequence, shown in Fig. 1 (a). The two complexes differ basically in their lithostratigraphic characteristics and are separated from each other by the Mahabharat Thrust (MT), which is the southern continuation of the MCT (Stocklin, 1980). On the other hand, the Lesser Himalayan rocks are thrust over the Siwaliks along with MBT.

The central region of Nepal is a seismo-tectonically active zone that was strongly shaken by the latest devastating 2015 Gorkha earthquake. Most devastating historical mega-earthquakes have been reported around the central part of the Nepal Himalaya (Chitrakar and Pandey, 1986; Bilham, 1995; Pandey et al., 1999). Numerous seismological studies (Molnar, 1984; Pandey et al., 1999; Bollinger et al., 2004; Hubbard et al., 2016; Yamada et al., 2020) have been carried out to explore the tectonic evolution and three-dimensional geometrical fault structure beneath central Nepal.

DATA SET

We selected 252 well located local earthquakes (Ml ≤ 4.8, epicentral distance 15-100 Km, and focal depth ≤ 25 Km) of central Nepal from NAMASTE network, using an earthquake catalog of Yamada et al. (2020) and vertical component seismograms (sampling frequency 100 Hz) of 16 different seismic stations were downloaded using BREQ_FAST request form from IRIS (https://ds.iris.edu/ds/nodes/dmc/forms/breqfast-request/) website. It is a temporary seismic network that was installed about seven weeks after the 2015 Gorkha earthquake. The network consisted of 41 broadband and short-period seismometers, and 14 strong-motion sensors at 46 sites across eastern and central Nepal (Karplus et al., 2020). We selected 16 seismic stations in this study, includes only broadband sensors (CMG3T, CMG-40T, and Nanometrics Trillium compact with Reftek 130 datalogger and Taurus standard 47 k as a digitizer) that were operating in the first phase of installation. Seismic Analysis Code (Goldstein and Snoke, 2005) is used to select the individual's station seismograms. Only good quality waveforms from downloaded data were selected and discarded those waveforms with poor signal to noise ratio, contaminated with other events, and counterfeit signals based on visual inspection. Fig. 1 (a) represents the selected local events and seismic station of this study. Most of the events are concentrated within the selected seismic network.

METHODOLOGY AND DATA ANALYSIS

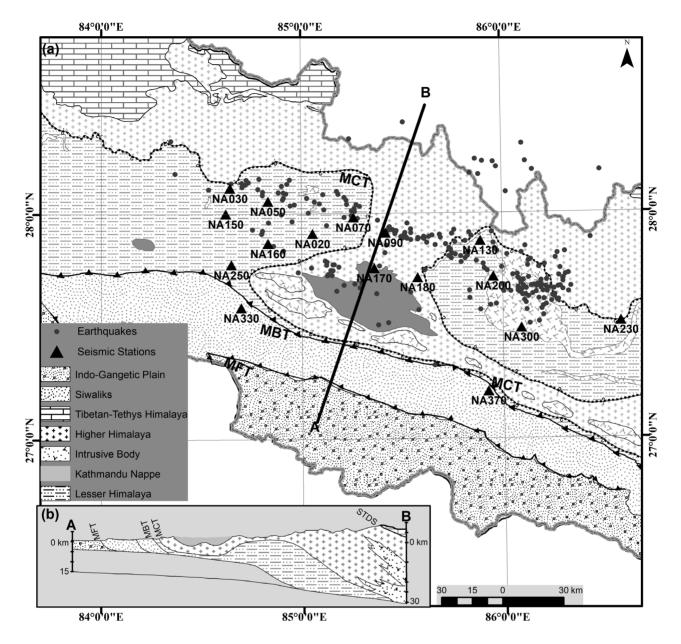Recently, various methods have been proposed to

Fig. 1: Location map of the study area. (a) Generalized geological map modified after Dahal (2006) with earthquake location and seismic stations. Black triangles represent the seismic stations. Black curves with small triangles and black dotted curves represent the faults. (b) Cross-section map with the major tectonic division of central Nepal (Pandey et al., 1999).

estimate the attenuation characteristics of coda waves. In this study, the program 'CodaQ' prepared by Kumar et al. (2015), is used for the estimation of attenuation characteristics of coda waves. This program is based on the well-known single backscattering model of Aki and Chouet (1975) and includes guidelines followed by SEISAN, EQK_SRC_PARA software (Havskov, and Ottemoller, 2005). In the single backscattering model, it is assumed that the coda wave is backscattered body waves generated by numerous heterogeneities of the lithosphere. Sato (1977) proposed a single isotropic scattering model for non-coincident source and receiver. From this model, coda wave amplitude, A (f,t) for central frequency 'f' over a narrow band width

signal and lapse time 't' measured from the earthquake origin time as follows (Aki, 1980):

$$A(f, t) = S(f)t^{-\alpha}\exp\left(\frac{-\pi ft}{Q_c}\right) \tag{1}$$

where S (f) represents the source function at central frequency 'f,' 'α' geometrical spreading factor taken as unity for body wave, and Qc is the quality factor representing the average attenuation (Intrinsic and scattering attenuation) characteristic of the media. The attenuation, due to geometrical spreading, is not included in Qc, is considered separately in equation (1). The logarithm of Eq. (1) is given in the following form:

$$\ln [A (f, t)] = \ln [S (f)] - \alpha \ln (t) - (\frac{\pi ft}{Q_c})$$

$$\ln [A (f, t)] + \alpha \ln (t) = \ln [S (f)] - (\frac{\pi ft}{Q_c})$$ (2)

Equation (2) represents the equation of the straight line in which [S (f)] is a constant, and the value of 'α' is unity. Then Eq. (2) becomes,

$$\ln [A (f, t)t] = C - (\frac{\pi f}{Q_c}) t$$ (3)

From Eq. (3), b = - π f/Q_c is the slope of the straight line, and C is constant. The Q_c can be obtained from linear regression analysis between ln[A (f, t)t] and lapse time for each central frequency.

The 1066 selected waveforms from 16 different seismic stations are used for this study. The using program 'CodaQ' requires Sesame ASCII File (SAF) format time series data for input data. Selected seismograms are converted to the SAF format by using the 'seisaf' sub-routine program of SEISAN

(Havskov and Ottemoller, 2005) before running the 'CodaQ.' P-wave and S-wave arrival time are marked individually on waveforms. Then an origin time of the event is calculated by the program using the relation, origin time =$\{t_p$ - 1.38 $(t_s$ - $t_p)\}$, shown in Fig. 2 (a). Each seismogram is filtered at eight different frequencies (Table 1) using the Butter-worth bandpass 4th order filter. Fig. 2 (b) shows band pass filtered seismogram at 1-2 Hz frequency.

Coda window length should be large to get a stable result. Havskov and Ottemoller (2005) suggested that the minimum value of the coda window length should be greater or equal to 20 s. We selected 4 different coda window length starting from 20 s. The length of the coda window of filtered seismograms is fixed at 20, 30, 40, and 50 s, starting from (twice of direct S-wave arrival) to eliminate contamination caused by direct S-wave (Rautian and Khalturin, 1978). The time of coda start ($2t_s$) is called lapse time. After then, each filtered seismogram is selected from coda arrival (TC) to coda arrival plus coda window (20, 30 s, etc.), shown in Fig. 2 (b). The amplitude of the selected
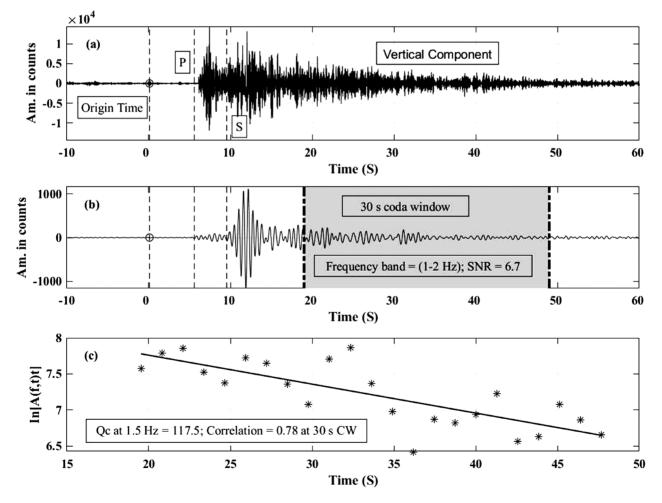

Fig. 2: Example of event processed (a) the high-frequency vertical component waveform at NA180 seismic station on 25/06/2015 (b) band pass filtered waveform with 30 s coda window length at 1-2 Hz frequency and (c) the RMS amplitude (plotting ln[A(f,t)t] versus lapse time) values multiplied with lapse time window at central frequency 1.5 Hz. The slope of this fitting line is the value of Q_c at given central frequency. P and S represent the P-wave and S-wave arrival time.

coda wave is multiplied by t^{-a} to account geometrical attenuation. Fig. 2 (c) displays the slope of the fitted straight line after plotting In[A (f, t) t] versus lapse time at 1.5 Hz central frequency. The root mean square (RMS) amplitudes of the selected coda wave are estimated using a moving time window of 2.56 s width with 1.28 s interval, shown in Fig. 2 (c). The value of coda Q at each central frequency is calculated using the slope fitted straight lines. The correlation coefficient for the fitted straight line (between In[A(f, t)t] and lapse time) for each central frequency is also measured to check the goodness of fitted straight line. Signal to noise ratio (S/N) is calculated from the last 5 seconds of the selected coda window for each central frequency for every record separately. Only waveforms with good S/N ratio (S/N ≥ 3) are included in the analysis to obtain reliable Q_C value.

The Q_C obtained using a large coda window represents the attenuation characteristic of the deeper lithosphere. Pulli (1984) has shown that the scatterers responsible for the generation of coda waves are generally assumed to be distributed over a surface area of an ellipsoid. The surface of an ellipsoid, whose surface projection is defined by the equation.

$$\frac{X^2}{(vt/2)^2} + \frac{Y^2}{(vt/2)^2 - (R/2)^2} = 1 \qquad (4)$$

where X and Y are the surface coordinates, and R is the distance between source and recording station. R is zero for the single backscattering model of Aki and Chouet (1975). The parameters v and t represent the velocity of S-wave and lapse time, respectively. Assuming the single backscatter model, the radius of the area where the coda wave was generated is

expressed as $vt/2$ (Mukhopadhyay and Tyagi, 2007). Based on this relationship, the radius of the area for each lapse time window is shown in Table 4, using the S-wave velocity of 3.71 km/s (Pandey et al., 1999; Yamada et al., 2020).

RESULTS AND DISCUSSION

The 1066 seismic waveforms of 16 different seismic stations were analyzed to calculate the coda wave quality factor, Q_C. The Q_C was estimated at eight different central frequency (Table 1) and four different coda windows from 20 to 50 s. The value of Q_C obtained from the analysis was filtered out with a signal to noise ratio of less than 3 and a correlation coefficient for the best fit line for the coda decay slope with respect lapse time of less than 0.6. These selected Q_C values are plotted as a function of frequency according to the relation $Q_C (f) = Q_0 f^n$, at each seismic station at each coda window length, shown in Table 2. 85 percent confidence interval is used to calculate the error range of Q_o and n. Table 2 shows the frequency-dependent relation for each station for each coda window length. Fig. 3 (a) and 3 (b) shows the spatial distribution of the Q_O and n values at each seismic station at 30 s coda window. The value of Q_O at NA090, NA230, NA330, NA030, and NA370 is relatively lower than in other stations, as shown in Fig. 3 (a). The stations NA330 and NA337 were installed on the sedimentary sequence of Siwalik zone, below MBT (Fig. 1 (a), but the remaining were installed on the metamorphic sequence of lesser and Higher Himalaya. The low Q_C values of these two may be due to change in the lithosphere beneath the stations. The seismic stations NA160, NA250, and NA150 have a relatively high value of Q_O, and less value of

Table 2: Frequency-dependent relation of Q_c at each seismic station at each lapse time window for a given frequency.

Station Name	Q_c at 20 sec.	Q_c at 30 sec.	Q_c at 40 sec.	Q_c at 50 sec.	N
NA020	79.7 ± 21.4 f ^1.11 ± 0.10	109.3 ± 15.3 f ^1.04 ± 0.05	145.9± 16.6 f ^0.95 ± 0.04	185.6 ± 19.8 f ^0.88 ± 0.04	106
NA030	67.4 ± 14.6 f ^1.17 ± 0.08	98.0± 19.6 f ^1.12 ± 0.07	161.6 ± 27.4 f ^1.00 ± 0.06	184.7± 29.9 f ^0.94 ± 0.06	54
NA050	69.6 ± 14.7 f ^1.18 ± 0.07	122.3 ± 26.5 f ^1.02 ± 0.08	170.7 ± 32.2 f ^0.92 ± 0.07	193.6 ± 30.2 f ^0.90 ± 0.06	63
NA070	83 ± 19.8 f ^1.05 ± 0.09	111.7 ± 13.4 f ^1.01 ± 0.04	147.7 ± 20.9 f ^0.94 ± 0.05	178.2± 24.4 f ^0.87 ± 0.05	81
NA090	59.5 ± 10.8 f ^1.14 ± 0.06	87.9 ± 10.4 f ^1.05 ± 0.04	139.8 ± 23.6 f ^0.89 ± 0.06	159.3 ± 16.1 f ^0.87 ± 0.04	91
NA130	56.2 ± 11.3 f ^1.24 ± 0.07	107.8 ± 20.0 f ^1.02 ± 0.07	170.1 ± 54.1 f ^0.87 ± 0.12	171.3 ± 60.3 f ^ 0.86 ± 0.13	58
NA150	98.9 ± 29.5 f ^1.03 ± 0.11	137.3 ± 27.6 f ^ 0.97 ± 0.07	159.1 ± 18.8 f ^0.94 ± 0.04	174.6 ± 18.3 f ^0.93 ± 0.04	51
NA160	84.4 ± 18.3 f ^ 1.03 ± 0.08	125.3 ± 14.9 f ^ 0.98 ± 0.04	164.1 ± 29.8 f ^ 0.90 ± 0.07	185.2 ± 21.1 f ^ 0.90 ± 0.04	75
NA170	66.4 ± 16.3 f ^ 1.17 ± 0.09	100.9 ± 12.8 f ^ 1.02 ± 0.05	119.0 ± 15.0 f ^ 0.99 ± 0.05	148.1 ± 14.0 f ^ 0.93 ± 0.03	73
NA180	84.4 ± 26.0 f ^ 1.08 ± 0.11	84.4 ± 26.0 f ^ 1.08 ± 0.11	112.5 ± 7.5 f ^ 1.00 ± 0.02	119.3 ± 13.0 f ^ 0.98 ± 0.04	48
NA200	70.4 ± 11.5 f ^ 1.13 ± 0.06	107.1± 14.5 f ^ 1.04 ± 0.05	165.9 ± 37.1 f ^ 0.87 ± 0.08	156.7 ± 25.1 f ^ 0.88 ± 0.06	71
NA230	86.5 ± 20.2 f ^ 1.01 ± 0.08	92.4 ± 12.7 f ^ 1.05 ± 0.05	95.4 ± 12.4 f ^ 1.08 ± 0.05	111.6 ± 19.0 f ^ 01.04 ± 0.06	77
NA250	89.8 ± 13.2 f ^ 1.05 ± 0.05	161.5 ± 29.9 f ^ 0.88 ± 0.07	206.3 ± 27.7 f ^ 0.84 ± 0.05	249.9 ± 40.2 f ^ 0.78 ± 0.06	71
NA300	72.8 ± 16.2 f ^ 1.12 ± 0.08	112.8 ± 23.9 f ^ 1.04 ± 0.08	144.9 ± 32.8 f ^ 0.96 ± 0.08	167 ± 30 f ^ 0.9 ± 0.06	90
NA330	64.9 ± 23.4 f ^ 1.12 ± 0.13	98.0 ± 23.9 f ^ 1.08 ± 0.09	115 ± 25.9f ^ 1.07 ± 0.08	171 ± 29.8 f ^ 0.96 ± 0.06	26
NA370	51.6 ± 6.7 f ^ 1.31 ± 0.05	92.0 ± 13.8 f ^ 1.11 ± 0.05	99.4 ± 15.3 f ^ 1.10 ± 0.05	106.5 ± 21.3 f ^ 1.09 ± 0.07	31
Mean Q_c	73.1 ± 10.1 f ^ 1.12 ± 0.05	110.0 ± 10.6 f ^ 1.03 ± 0.03	143.5 ± 14.2 f ^ 0.95 ± 0.04	156.1 ± 13.6 f ^ 0.92 ± 0.03	1066

N: Number of seismograms used in the analysis

n, as compared to other stations at 30 s coda window, shown in Table 2, Fig. 3 (a), and 3 (b). The Q_c of each station shows the spatial variation of attenuation in the study area, a similar result obtained in the southern Tibet to eastern Nepal (Biswas and Singh, 2019).

Table 2 shows that the Q_c values increase, and the *n* values decrease, with increases in coda window length for all central frequencies except a station NA230. The station NA230 has relatively low Q_c values, and the *n* values increase with an increase

in the coda window. It may be happened due to high intrinsic attenuation (Yavuz and Baris, 2019). The Q_c values have been reported significantly lower at thermal springs, volcanic structure, and high magmetic activity Havskov et al., 1989; Canas et al., 1995; Naghavi et al., 2017) than its surrounding areas. Yavuz and Baris (2019) reported that both the values of Q_c and *n* increase with an increase in lapse time in the thermal spring area. Intrinsic attenuation is sensitive to physical conditions (geothermal activity) of the underlying medium while scattering attenuation
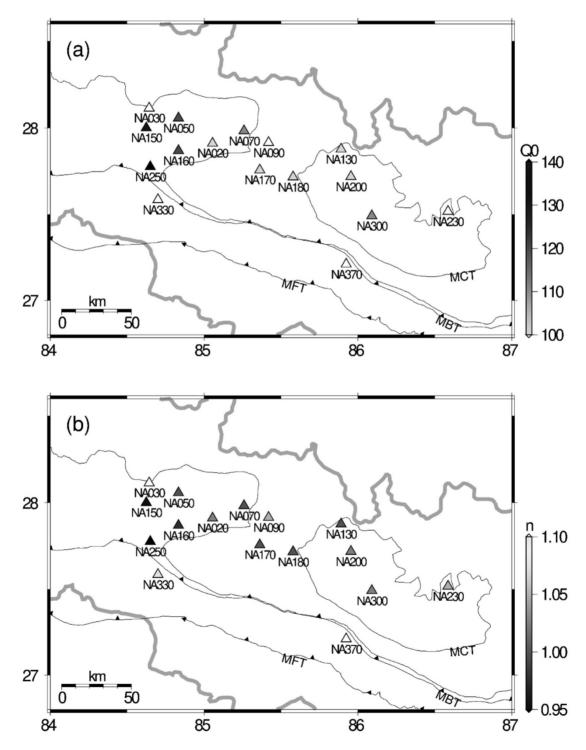

Fig. 3: Spatial distribution of (a) Qo and (b) n values at each seismic station at 30 s coda window. The MFT, MBT, and MCT are the major fault systems in this region. The triangles represent the seismic stations.

indicates the degree of heterogeneities (Sato and Sacks, 1989).

The mean Q_c values of this region for four different coda windows are calculated by averaging all these stations's Q_c values (Table 3). We obtained the mean values of Q_c is $110 \pm 10.6\,f^{\,1.03\pm0.03}$ at 30 s coda window. Fig. 4 shows the mean Q_c obtained from four different coda window length. The value of Q_O from the mean of all stations, increases with increases in coda window length and the value of *n* decreases with increasing the coda window for all central frequency, shown in Table 4. The Q_c values at 1.5 Hz for all coda wondows are lower than the regression line, shown in Fig. 4. It may occur due to the presence of backscattering of surface waves from low Q part of the earth's crust or contamination of low-velocity surface waves at the initial part of the coda waves. The coda waves at around 1 Hz can not be explained as backscattering body waves from heterogeneities in the lithosphere; they are backscattering surface waves from heterogeneities in the lithosphere (Aki and Chout, 1975).

Frequency-dependent Q_c is interpreted as a tectonic parameter (Paul et al., 2003). It depends on both degree of tectonic activity in an area and level of heterogeneity of a medium (Aki, 1980; Roecker et al.,
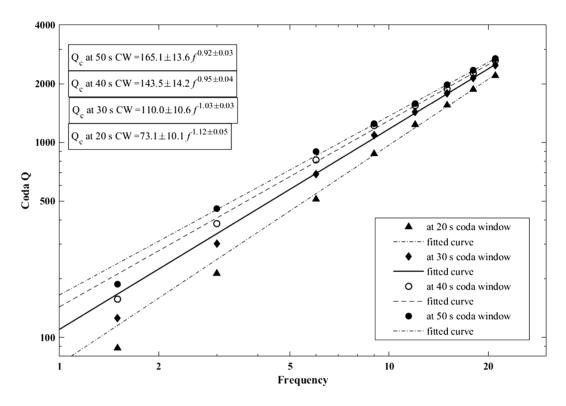

Fig. 4: Graphical representation of the frequency-dependent relation of mean Q_c with model correlation at four different coda window length from 20 to 50 s.

Table 3. Mean value of Q_c and number of observations at each central frequency at each lapse time.

Frequency (Hz)	20 Sec. window length		30 Sec. window length		40 Sec. window length		50 Sec. window length	
	Q_c	N	Q_c	N	Q_c	N	Q_c	N
1.5	88.145	447	125.3031	394	157.1169	311	187.4575	307
3	212.8421	512	301.9088	489	383.1469	429	457.49	443
6	511.0544	449	686.3219	494	812.8356	515	897.2288	508
9	873.9938	531	1088.653	616	1218.866	538	1246.973	497
12	1233.029	529	1430.856	562	1544.195	488	1581.592	412
15	1552.675	487	1781.297	510	1878.642	427	1977.799	373
18	1870.016	456	2134.109	484	2263.378	401	2347.086	343
21	2199.763	421	2494.624	446	2629.893	358	2694.146	286

N: total number of observations made for each central frequency

Table 4: Q_o (quality factor at 1 Hz) and n values with standard deviations at different coda window length and the maximum radius of area of coda generation.

Coda window length (S)	Q_o value	n value	Radius of spherical surface (Km)
20	73.1 ± 10.1	1.12 ± 0.05	37.1
30	110 ± 10.6	1.03 ± 0.03	55.6
40	143.5 ± 14.2	0.95 ± 0.04	74.2
50	156.1 ± 13.6	0.92 ± 0.03	92.75

1982; Singh et al., 2012). According to Aki (1980), the lower Q_C values for lower frequencies may show a high degree of heterogeneity, whereas high Q_C values for higher frequencies may be related to relatively more homogenous deeper layers.

Table 4 shows the approximate radius of medium contributing to coda generation, which increases with increasing coda window. The increase in Q_C values with coda window has also been interpreted as a function of depth by many investigators (Gupta et al., 1996; Havskov, 1989; Roecker et al., 1982; Woodgold, 1994). It is concluded that an increase in Q_C values with increasing coda windows at a given frequency indicates an increase in Q_C with increasing depth. It means that coda attenuation decreases with increasing depth of the study area.

Table 4 shows that Q_O, from the mean of all stations, increases with increases in coda window length and the value of n decreases with increasing the coda window for all central frequency which is similar to finding for several others regions (e.g., Ibanez et al., 1990; Kosuga, 1992; Wooggold, 1994; Gupta et al., 1998; Yoshimoto and Jin, 2008; Calvet and Margerin, 2013). Woodgold (1994) also included the other factors that affect the increase in Q_C with increasing coda window, such as (i) multiple scattering is significant and (ii)

consideration of non-zero source to receiver distance with non-isotropic scattering. According to Gao et al. (1983), the effect of multiple scattering becomes insignificant for local events with a coda window of less than 100 s. In this analysis, the length of coda window has been chosen up to 50 s (less than 100 s) and the starting time of the coda wave for coda window has been taken twice of the S-wave travel time (Aki and Chouet, 1975) to avoid all direct wave (Rautian and Khalturin, 1978) and minimize the effect of the second assumption of Woodgold (1994). According to Aki and Chout (1975), the backscattering of surface waves is contaminated as a coda at around 1 Hz in the shallow lithosphere. Higher frequency coda is not contaminated by the backscattering of surface waves. From the above discussion, the result of this study shows the lapse time dependence of coda Q.

Table 5 shows the frequency-dependent coda Q of some tectonically active and stable regions of the world. According to Kumar et al. (2014), the higher value of n indicates high tectonic activity. Therefore, the degree of frequency dependence, n, represents the level of tectonic activity of the region. The Q_O of New England and south India is relatively greater, and the n value of these regions is relatively smaller than the other regions in Table 5. These two represent

Table 5: Frequency-dependent $Q(f)$ relationship for some active and stable regions of the world.

Region	Relation	Reference
Central region (Nepal)Garhwal Himalaya	$110 f^{1.03}$	Present study
	$125 f^{0.95}$	Gupta et al. (1995)
Kumaon Himalaya	$92 f^{1.07}$	Paul et al. (2003)
Western Nagao, Japan	$112 f^{0.67}$	Kosuga (1992)
Mainland Gujarat	$87 f^{1.01}$	Gupta et al. (2012)
Koyna region (India)	$117 f^{0.97}$	Sharma et al. (2007)
Washington state (USA)	$63 f^{0.97}$	Havskov et al. (1989)
South India	$460 f^{0.83}$	Mandal & Rastogi (1998)
New England	$460 f^{0.4}$	Pulli (1984)
Northwestern Himalaya	$158 f^{1.05}$	Kumar et al. (2005)
Friuli, Italy	$80 f^{1.1}$	Rovelli (1982)
South Spain	$155 f^{0.89}$	Ibanez et al. (1990)
Northern Morocco	$97.58 f^{0.96}$	Boulanouar et al. (2017)
Turkey	$77 f^{0.8}$	Yavuz and Baris (2019)

the seismo-tectonically stable regions. The value of n(=1.03 at 30 s coda window) in our study is similar to these results in the tectonically active regions (Rovelli, 1982; Gupta et al., 1995; Hellweg et al.,1995). We compared the Q_c estimated in this study with the result obtained from two different active regions (Himalayan regions near the study area and others tectonically active regions in the world) of the world at 30 s coda window, respectively, shown in Fig. 5 (a) and 5 (b). Fig. 5 (a) shows that the attenuation of the present study's coda wave is almost similar to the Garhwal, Kumaon and Koyna regions and higher than the Northwestern Himalaya, India. Most of the events are concerned around the vicinity of the well known MBT and MCT discontinuities in our study

and almost similar tectonic setting and somehow different in lithology and structure with Garhwal, Kumaon, Koyna regions and Northwestern Himalaya (Gupta et al., 1995; Paul et al., 2003; ; Kumar et al., 2005; Sharma et al., 2007). Mainland Gujarat is more attenuating than our study: the Mainland Gujarat is dominated by Terai regions (Gupta et al., 2012).

Fig. 5 (b) shows that the coda Q obtained in the present study is higher than Italy, Northern Morocco, Washington, western Nagano, and Turkey and almost similar to Southern Spain. Relatively less value of coda Q is observed in geothermal activities and hotspot in the different regions of the world (Havskov et al. 1989; Canas et al. 1995; Naghavi et al. 2017).
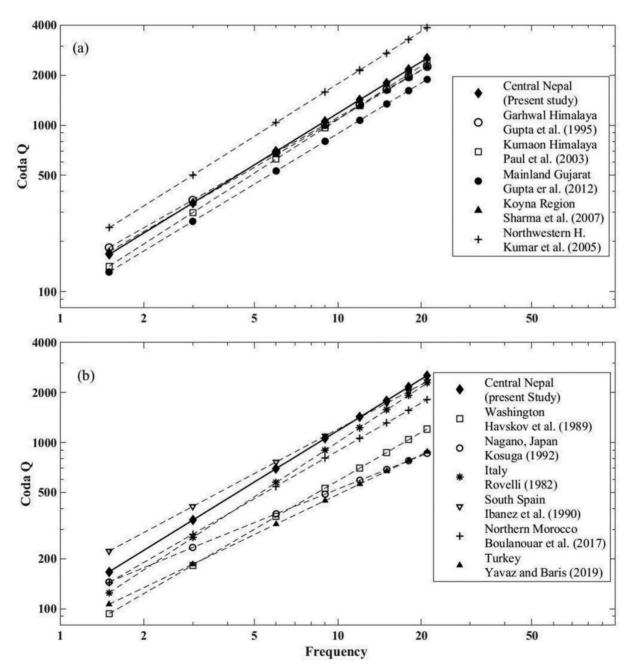

Fig. 5: Comparison of Q_c values for the central region of Nepal Himalaya, with active (a) Himalaya regions near the target of this study and (b) others tectonically active regions in the world.

83

The values of Q_C have been reported significantly lower in Turkey due to thermal springs (Yavuz and Baris, 2019), in Washington due to volcanic structure (Havskov et al., 1989) than its surrounding areas. The Q_C and *n* obtained in this study are compatible with the results having a similar tectonic setting of the other active regions of the world, shown in Table 5.

CONCLUSIONS

The attenuation characteristic of the central region of Nepal Himalaya is described with the help of the coda wave. The frequency-dependent (from 1.5 to 21 Hz) relationship for coda wave quality factor (Q_C)has been estimated using four different coda window lengths. We obtained the mean values of Q_C is $110\pm10.6\ f$ $^{1.03\pm0.03}$ at 30 s coda window. The estimated mean values of Q_C and their high-frequency dependent relationship indicate that the medium of the central region (the study area) is highly heterogeneous and seismo-tectonically active. The increase in Q_C with an increase in coda window from 20 to 50 s indicates the lapse time dependence of coda Q. The value of Q_O and *n* obtained at 30 s coda window in this study are compatible with the results obtained in having a similar tectonic setting of the other active regions of the world. The frequency-dependent relations established here are useful for earthquake source parameters.

AUTHOR'S CONTRIBUTIONS

P. Pokhrel conducted the statistical analysis and designed the tables. T.P. Kandel collected, processed, and analyzed the seismic data. P. Pokhrel and T.P. Kandel drafted the figures and the manuscript. M. Yamada supervised the data processing and data analysis, and interpreted the results. All authors contributed to the final version of the manuscript.

REFERENCES

Aki, K., 1969, Analysis of the seismic coda of local earthquakes as scattered waves. Journal of Geophysical Research,74, 615-631.

Aki, K., 1980, Attenuation of shear waves in the lithosphere for frequencies from 0.05 to 25Hz. Physics of the Earth and Planetary Interiors, 21, 50-60.

Aki, K. and Chouet, B., 1975, Origin of the coda waves: source, attenuation and scattering effects. Journal of Geophysical Research, 80, 3322-3342.

Avouac, J.P., 2003, Mountain Building, Erosion, and the Seismic Cycle in the Nepal Himalaya. Advances in Geophysics, Vol. 46, 10.1016/S0065-2687(03)46001-9.

Bilham, R., 1995, Location and magnitude of the 1833 Nepal earthquake and its relation to the rupture zones of contiguous great Himalayan earthquakes. Curr. Sci., 69, 101–128.

Biswas, R. and Singh, C., 2019, Lateral variation of crustal attenuation properties from southern Tibet to eastern Nepal Himalaya. Geophys. J. Int., 217, 257-270.

Bollinger, L., Avouac, J.P., Cattin, R., and Pandey, M.R., 2004, Stress buildup in the Himalaya. Journal of Geophysical Research, 109, B11405, doi:10.1029/2003JB002911.

Boulanouar, A., Moudnib, L.E., Padhy, S., Harnafi, M., Villasenor, A., Gallart, J., Pazos, A., Rahmouni, A., Boukalouch, M., and Sebbani, J., 2017, Estimation of coda wave attenuation in northern Morocco. Pure Appl. Geophys, 1724-4.

Calvet, M. and Margerin, L., 2013, Lapse-time dependence of coda Q: Anisotropic multiple scattering models and application to the Pyrenees. Bull. Seis. Soc. Am., 103(3), 1993-2010.

Canas, J.A., Pujades, L.G., Blanco, M.J., Soler, V., and Carracedo, J.C., 1995, Coda-Q distribution in the Canary Islands. Tectonophysics, 246, 245-261.

Cattin, R. and Avouac, J., 2000, Modeling mountain building and the seismic cycle in the Himalaya of Nepal. J. Geophys. Res., 105, 13,389–13,407.

Chitrakar, G.R. and Pandey, M.R., 1986, Historical earthquake of Nepal. Bull. Geol. Soc. Nepal, 4, 7-8.

Dahal, R., 2006, Geology for Technical Students. Bhrikuti Academic Publication, Kathmandu, Nepal. 756 pp.

Gao, L.S., Lee, L.C., Biswas, N.N., and Aki, K.,

1983, Comparison of the single and multiple scattering on coda waves for local earthquakes. Bulletin of the Seismological Society of America, 73, 377–389.

Goldstein, P. and Snoke, A., 2005, SAC Availability for IRIS Community. Incorporated Research Institutions for Seismology Data Management Center Electronic Newsletter, VII, 1.

Gupta, S.C., Singh V.N., and Kumar, A., 1995, Attenuation of coda waves in the Garhwal Himalaya, India. Phys Earth Planet Inter, 87, 247–253.

Gupta, S.C., Kumar, A., Singh, V.N., and Basu, S., 1996, Lapse-time dependence of Qc in the Garhwal Himalaya. Bull Indian Soc.Earthq. Technol., 33:147–159.

Gupta, S.C., Teotia, S.S., Rai, S.S., and Gautam, N., 1998, Coda Q estimates in the Koyna region, India. Pure Appl. Geophys., 153:713–731.

Gupta, S.C. and Kumar, A., 2002, Seismic wave attenuation characteristics of three Indian regions, a comparative study. Curr. Sci. 82, 407–413.

Gupta, A.K., Kumar, A., Chopra, S., Kumar, S., and Rastogi, B.K., 2012, Attenuation Characteristics of Coda Waves in Mainland Gujarat (India). Tectonophysics, V., 530-531, 264-271.

Havskov, J., Malone, S., McClurg, D., and Crosson, R., 1989, Coda Q for the state of Washington. Bulletin of the Seismological Society of America, 79, 1024-1038.

Havskov, J. and Ottemoller, L., 2005, SEISAN (version 8.1): The earthquake analysis software for Windows, Solaris, Linux, and Mac OSX Version 8.0. pp 254.

Hellweg, M., Spandich, P., Fletcher, J.B., and Baker, L.M., 1995, Stability of coda Q in the region of Parkfield, California: view from the U.S. Geological Survey Parkfield Dense Seismograph Array. Journal of Geophysical Research.,100, 2089–2102.

Hubbard, J., Almeida, R., Foster, A., Sapkota, S.N., Burgi, P., and Tapponnier, P., 2016, Structural segmentation controlled the 2015 Mw 7.8 Gorkha earthquake rupture in Nepal. Geology, 44(8), 639–642.

Ibanez, J.M., Del pezzo, E., De Miguel, F., Herraiz, M., Alguaicil, G., and Morales, J., 1990, Depth dependent seismic attenuation in the Granada zone (southern Spain). Bull Seism Soc Am 80:1232–1244.

International Federation of Digital Seismograph Networks, https://www.fdsn.org /networks/detail/XQ_2015.

IRIS Data Management Center, https://ds.iris.edu/ds/ nodes/dmc/forms/breqfast-request/.

Kanao, M. and Ito, K., 1991, Attenuation of S waves and coda waves in the inner zone of southwestern Japan. Bull. Disas. Prev. Inst., Kyoto Univ., 41(2).

Karplus, M.S., Pant, M., Sapkota, S.N., Nabelek, J.L., Velasco, A.A., Adhikari, L.B., Ghosh, A., Klemperer, S.L., Kuna, V., Mendoza, M., and Braunmiller, J., 2020, A rapid response network to record aftershocks of the 2015 M 7.8 Gorkha earthquake in Nepal. Seismological Research Letters, online.

Kosuga, M., 1992, Dependence of coda Q on frequency and lapse time in the western Nagano region, central Japan. J. Phys. Earth, 40, 421-445.

Kumar, A., Sinvhal, A., Joshi, A., Kumar, D., and Kumar, P. K., 2014, Coda wave attenuation characteristics for Kumaon and Garhwal Himalaya, India. Natural Hazards, 75, 1057-1074.

Kumar, A., Kumar, R., Ghangas, V., and Sharma, B., 2015, MATLAB codes (CodaQ) for estimation of attenuation characteristics of coda waves. International Journal of Advanced Research, 3, 1078-1083.

Kumar, N., Parvez, I., and Virk, H., 2005, Estimation of coda wave attenuation for NW Himalayan region using local earthquakes. Physics of the Earth and Planetary Interiors, vol. 151, 243-258.

Mandal, P. and Rastogi, B.K., 1998, A frequency-dependent relation of coda Qc for Koyna-Warna region India. Pure Appl. Geophys., 153, 163–177.

Molnar, P., 1984, Faulting associated with large earthquakes and the average rate of deformation in central and eastern Asia. Journal of Geophysical Research, 89,6203-6227.

Molnar, P. and Tapponnier, p., 1975, Cenozoic tectonics of Asia: Effects of a continental collision. Science, 189, 419 – 426.

Mukhopadhyay, S. and Tyagi, C., 2007, Lapse time and frequency dependent characteristics of coda in the Northwestern Himalayas. Journal of Seismology, 11, 149-158.

Naghavi, M., Rahimi, H., Moradi, A., and

Mukhopadhyay, S., 2017, Spatial variations of seismic attenuation in the North West of Iranian plateau from analysis of coda waves. Tectonophysics, 708, 70-80.

Pandey, M.R., Tandukar, R.P., Avouac, J.P., Vergne, J., and Heritier, T., 1999, Seismotectonic of the Nepal Himalaya from a local seismic network. Jour. Asian Earth Sciences, 17, 703–712

Paul, A., Gupta, S.C., and Pant, C.C., 2003, Coda Q estimates for Kumaon Himalaya. Earth Planet Sci 112, 569–576.

Pulli, J.J., 1984, Attenuation of coda waves in New England. Bulletin of the Seismological Society of America, 74, 1149-1166.

Rautian, T.G. and Khalturin, V., 1978, The use of coda for determination of the earthquake source spectrum. Bulletin of the Seismological Society of America, 68, 923-948.

Roecker, S.W., Tucker, B., King, J., and Hatzfield, D., 1982, Estimates of Q in central Asia as a function of frequency and depth using the coda of locally recorded earthquakes. Bull. Seismol. Soc. Am., 72, 129–149.

Rovelli, A., 1982, On the frequency dependence of Q in Friuli from short-period digital records. Bulletin of the Seismological Society of America, 72, 6, 2369-2372.

Sato, H., 1977, Energy propagation including scattering effects: Single isotropic approximation. J. Phys. Earth, 25, 27-41.

Sato, H., Fehler, M.C., and Maeda, T., 2012, Seismic wave propagation and scattering in the heterogenous earth. Springer-verlay Berlin Heidelberg, second edition, 80-82.

Sato, H. and Sacks, I.S., 1989, Anelasticity and thermal structure of the oceanic upper mantle: Temperature calibration with heat flow data. Journal of Geophysical Research: Solid Earth, 94.B5, 5705-5715.

Sharma B, Teotia S.S., and Kumar, D., 2007, Attenuation of P, S and coda waves in Koyna region, India. J Seism 11:327–344.

Singh, C., Singh, A., Bharathi, V.K., Bansal, A.R., and Chadha, R.K., 2012, Frequency dependent body wave attenuation characteristic in the Kumaun Himalaya. Tectonophysics, 524-525, 37-42.

Stein, S. and Wysession, M., 2009, An Introduction to Seismology, Earthquakes, and Earth Structure, Chapter 4: Earthquakes. Wiley-Blackwell Publishing, p185-198.

Stöcklin, J. and Bhattarai, K.D., 1977, Geology of the Kathmandu area and central Mahabharat range, Nepal Himalaya. Report of Department of Mines and Geology/UNDP (unpublished), 86 p

Stöcklin, J., 1980, Geology of Nepal and its regional frame. Jour. Geol. Soc. London, v. 137, pp. 1-34.

Tripathi, J. N., Singh, P., and Sharma, M.l., 2012. Variation of seismic coda wave attenuation in the Garhwal region, Northwestern Himalaya. Pure and Applied Geophysics, 169,71-88.

Woodgold, C.R.D., 1994, Coda Q in the Charlevoix, Quebec region: lapse-time dependence and spatial and temporal comparison. Bulletin of the Seismological Society of America, 84, 1123–1131.

Yamada, M., Kandel, T., Tamaribuchi, K., and Ghosh, A., 2020, 3D fault structure inferred from a refine aftershock catalog for the 2015 Gorkha earthquake in Nepal. Bulletin of the Seismological Society of America, 110, 26-37.

Yavuz, E. and Baris, S., 2019, Determination of coda wave attenuation characteristic of the Armutlu Peninsula and its surrounding (Middle Marmara, Turkey). Annals of Geophysics, 62.

Yoshimoto, K. and Jin, A., 2008, Coda energy distribution and attenuation. Advances in geophysics, 50, 265-299.